INTERNATIONAL JOURNAL FOR NUMERICAL METHODS IN FLUIDS, VOL. 21, 1137–1151 (1995)

NUMERICAL SIMULATION OF TRANSIENT PLANAR FLOW OF A VISCOELASTIC MATERIAL WITH TWO MOVING FREE SURFACES

WENQUN MAO

Department of Mathematics and Statistics, McGill University, Burnside Hall, 805 Sherbrooke St. West, Montreal, QC, Canada H3A 2K6

AND

ROGER E. KHAYAT*

National Research Council of Canada, Industrial Materials Institute, 75 de Mortagne Blvd., Boucherville, QC, Canada J4B 6Y4

SUMMARY

In this study, we examine the numerical simulation of transient viscoelastic flows with two moving free surfaces. A modified Galerkin finite element method is implemented to the two-dimensional non-steady motion of the fluid of the Oldroyd-B type. The fluid is initially placed between two parallel plates and bounded by two straight free boundaries. In this Lagrangian finite element method, the spatial mesh deforms in time along with the moving free boundaries. The unknown shape of the free surfaces is determined with the flow field u, v, τ, p by the deformable finite element method, combined with a predictor–corrector scheme in an uncoupled fashion. The moving free surfaces and fluid motion of both Newtonian and non-Newtonian flows are investigated. The results include the influence of surface tension, fluid inertia and elasticity.

KEY WORDS: transient planar flow; viscoelastic material

1. INTRODUCTION

A *free boundary*, or *free surface*, problem is defined as a boundary value problem involving partial differential equations on domains in which the locations of the free boundary or boundaries are unknown. The unknown boundaries are called the free boundaries and they must be determined as part of the solution to the boundary value problem. A *moving boundary* problem is an initial value problem involving time-dependent, i.e. moving, free boundaries. A wide variety of physical phenomena involve moving free surfaces: e.g. jets,[1] water waves,[2] cavities,[3] and material forming processes.[4] One of the most challenging tasks is to develop efficient numerical algorithms for tracking moving free surfaces.[5,6] A comprehensive account of numerical methods and techniques for treating Newtonian free surface flow problems may be found in the reviews by Yeung[2] for inviscid flows and more recently by Floryan and Rasmussen.[7] Free surfaces are intrinsic parts of any shape changing process. When non-Newtonian flows involve a free surface, the solution becomes even more difficult to obtain. Examples of non-Newtonian flows, in particular viscoelastic flows, are encountered in the area of polymer processing which has been rapidly developing in the plastics industry.

One must acknowledge that the general characterization of non-Newtonian behaviour, by means of a functional constitutive equation, does not lead to tractable equations in any but the simplest of flow problems. Furthermore, even allowing for the significant simplfication that often results from a consideration of certain restricted classes of flows, the governing equations can still be much more

*Author to whom correspondence should be addressed.

CCC 0271–2091/95/121137–15

Received June 1994
Revised April 1995

complicated in detail than the Navier–Stokes equations. This means that most flow problems in non-Newtonian fluid mechanics are more demanding from the numerical techniques point of view, and progress has been largely dependent on the speed and storage capacity of available computers.

In material forming processes, such as film blowing[8] or extrusion,[9] the flow is steady and involves only one free surface. Steady viscoelastic flow problems with only one free surface are already so difficult to solve that one may easily predict the increased complexity and major computational cost associated with the addition of transient behaviour and another free surface. For example, flows with two moving free surfaces are relevant to blow molding and gas-assisted injection molding.[10,11] Comprehensive reviews of available numerical techniques and published numerical simulation can be found in References 12–14 and 4. However, the problem of transient viscoelastic flow with two moving free surfaces remains challenging and unsolved. Serious progress will have to be made on the efficiency of the algorithms before one can afford the calculation of transient viscoelastic flows with two free boundaries. In this regard, Khayat[15] gave a perturbation approach and examined the influence of fluid elasticity and that of surface tension.

Three aspects arise in the numerical treatment of a transient viscoleastic free surface flow problem: (1) the discrete representation for the flow field and free surfaces; (2) its approximated evolution in time; and (3) the manner in which the unknown variables are solved and the free surface location is determined. Concerning the third aspect, most work on free surface flows is divided into two basic approaches. In the first approach, since the location of the free surface is an additional degree of freedom, one more equation is needed in comparison with conventional problems with fixed boundaries. This additional equation can be solved as part of the complete system of nonlinear partial differential equations, including the additional dependent variable, i.e. location of the free surface. This is a coupled approach.[16,17] The second approach is the successive approximation method which uses a correction rule to modify the free surface shape. This is an uncoupled approach which was deveoped by Nichell *et al.*[8] and also be Ryskin and Leal.[19] Recently, similar techniques have been developed for various types of free surface problems.[20,3,21] The uncoupled approach is easier to implement and will be used in this work.

Adaptive methods using deforming finite element meshes were developed in the early 1980s for solving a broad range of moving boundary problems. A conceptual framework for this technique has been established by Lynch.[22,23] A similar algorithm is implemented in the present work for solving the transient viscoelastic flow with two free surfaces. The numerical procedure is based on the Galerkin finite element method on the deformable mesh, combined with a finite difference scheme in time. The Newton–Raphson iteration scheme is used to solve the resulting non-linear algebraic system of equations. The location of the free surfaces is determined by solving the kinematic boundary conditions at the two surfaces. A predictor–corrector method is used to locate the free surfaces after the flow field is determined. The method is applied to two-dimensional incompressible viscoelastic fluid contained between two parallel plates. The fluid is initially bounded by two straight free surfaces. The motion is set by the action of a driving pressure difference. The results obtained in the present study include both Newtonian and viscoelastic flows of the Oldroyd-B type. The effects of inertia, surface tension and elasticity are investigated. The results are relevant to the development of a reaslistic simulation and optimization of some polymer processing operations, in particular, blow molding and gas-assisted injection molding.

2. PROBLEM FORMULATION

Classical fluid dynamics is based on Newton's law which defines the viscosity of a fluid as the coefficient of proportionality between the shear stress and the velocity gradient. Newton's equation has been found to be successful in describing the flow phenomena of gases and liquids made up of small

molecules. However, polymeric fluids behave quite differently from liquids made up of small molecules. They do not obey the law of classical (Newtonian) fluid dynamics.[24] A fluid that does not behave in accordance with Newton's law is called a non-Newtonian fluid. Non-Newtonian fluid mechanics differ from classical Newtonian fluid mechanics in many important aspects. One of the most important differences is that the constitutive equation of non-Newtonian fluids varies from one flow type to another, which results in different governing equations, whereas in the classical situation the Navier–Stokes equations are accepted without question as governing equations.

In the present work, the Oldroyd-B model is used as the constitutive equation for the non-Newtonian flow. It has been frequently used for developments in numerical simulation of polymeric flows. It has shown good predictive ability in some polymeric flows. Simultaneously, it has been found that the flow of such fluids is one of the most difficult models to simulate among the set of available constitutive equations. In this sense, the model has helped considerably in the development of numerical algorithms for modelling viscoelastic flow.

The problem we consider is described in Figure 1. The initial geometry is taken to be a rectangle which contains the viscoelastic fluid between two parallel plates, with two straight free surfaces located at $x = R_1$ and $x = R_2$. The fluid is forced to deform under the action of applied external pressure. The fluid is assumed to adhere to the two plates so that the no-slip boundary condition holds at $y = 0$ and $y = L$, L being the distance between the two plates. In the following section, the governing equations as well as the boundary conditions for the problem will be presented.

2.1. *Governing equations*

The motion of the fluid is dictated by the equations of conservation of mass and momentum. Compressibility effects can be neglected in most applications. These equations are written in terms of the flow velocity $\mathbf{v}$, pressure p and stress τ. Thus the continuity and momentum equations are

$$\nabla \cdot \mathbf{v} = 0, \tag{1}$$

$$\rho \frac{\mathrm{D}\mathbf{v}}{\mathrm{D}t} = -\nabla p + \nabla \cdot \tau + \mathbf{f}, \tag{2}$$

where ρ denotes the density, $\mathbf{f}$ is any body force per unit volume, and $\mathrm{D}/\mathrm{D}t$ is the material derivative.

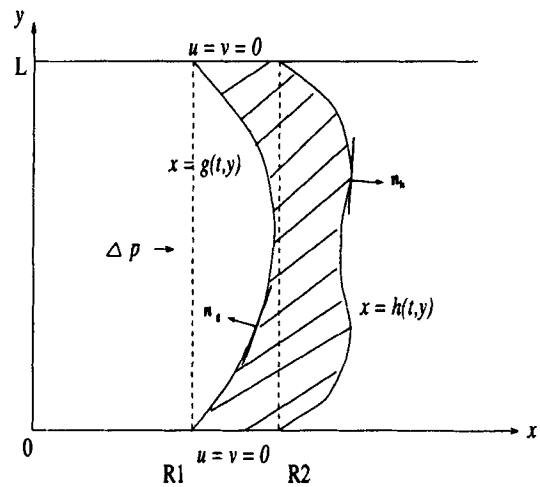

Figure 1. Transient viscoelastic flow with two free surfaces represented by the height functions g and h. Initial flow domain shown between the two dashed lines

The first major question posed in the simulation of a specific viscoelastic problem is the selection of a constitutive equation. A large body of established knowledge is available for the selection of appropriate constitutive equations. It should be pointed out that the identification of a suitable constitutive equation for polymer processing simulation is an unsolved problem. In this work, the viscoelastic nature of the fluid is introduced through the Oldroyd-B constitutive equation, for which the stress τ is given as the sum of elastic and Newtonian contributions:

$$\tau = \tau_1 + \tau_2. \tag{3}$$

The second term is the Newtonian contribution to the stress and is equal to

$$\tau_2 = 2\mu_2 \mathbf{D}, \tag{4}$$

where $\mathbf{D}$ is the rate-of-strain tensor and μ_2 is the solvent viscosity. The polymeric contribution to the stress is given by the term τ_1 which satisfies the upper-convected Maxwell equation:

$$\tau_1 + \lambda_1 \overset{\nabla}{\tau}_1 = 2\mu_1 \mathbf{D}, \tag{5}$$

where the upper-convected derivative is defined as

$$\overset{\nabla}{\tau}_1 = \frac{\mathrm{D}\tau_1}{\mathrm{D}t} - (\nabla \mathbf{v})^{\mathrm{T}} \cdot \tau_1 - \tau_1 \cdot \nabla \mathbf{v}, \tag{6}$$

μ_1 is the polymeric contribution to the shear viscosity, and λ_1 is the polymer relaxation time.

It is remarked that the Oldroyd-B model describes the rheological behaviour of dilute solutions of flexible, high molecular mass polymer in very viscous Newtonian solvents, even when these fluids are highly elastic. The model does not predict shear thinning. With only three material parameters, it is easy to understand, and has been able to represent a number of macroscopic observations in polymer fluids.

Upon elimination of τ_2 in the momentum equation (2), and only (5) being needed as the stress equation, we obtain a set of non-linear partial differential equations as governing equations

$$\rho \frac{\mathrm{D}\mathbf{v}}{\mathrm{D}t} = -\nabla p + 2\mu_2 \nabla \cdot \mathbf{D} + \nabla \cdot \mathbf{T} + \mathbf{f}, \tag{7}$$

$$\mathbf{T} + \overset{\nabla}{\mathbf{T}} = 2\mu_1 \mathbf{D}, \tag{8}$$

$$\nabla \cdot \mathbf{v} = \mathbf{0}, \tag{9}$$

to be solved for $\mathbf{v}$, $\mathbf{T}$, p in a flow domain $\Omega(t)$, where $\mathbf{T} \equiv \tau_1$. For the transient flow, the unknown fields depend on the time t and the position vector $\mathbf{x}$, i.e. $\mathbf{v}(t, \mathbf{x})$, $\tau_1(t, \mathbf{x})$ and $p(t, \mathbf{x})$.

As special cases, if

$$\lambda_1 = \mu_1 = 0,$$

then $\mathbf{T}$ vanishes, and the above set of partial differential equations (7)–(9) reduces to Navier–Stokes equations; if

$$\mu_2 = 0,$$

then we obtain the equations for upper-convected Maxwell fluid.

2.2. Boundary conditions

In the presence of two free surfaces, the flow domain $\Omega(t)$ is an unknown function of time. We need additional boundary conditions to determine the location of the free surfaces. A simple way of representing a free surface is to define its distance from a reference line as a function of position along

the reference line. We assume that Ω is two-dimensional, and that its inner and outer free surfaces can be represented by height functions of time and a single space co-ordinate $x = g(t, y)$, $x = h(t, y)$ (see Figure 1). In this case, the evolution of the deforming flow domain, i.e. the height functions, can be determined through kinematic conditions. This expresses the fact that the surfaces must move with the fluid,

$$\frac{\partial g}{\partial t} + v(t, g, y)\frac{\partial g}{\partial y} = u(t, g, y), \tag{10}$$

$$\frac{\partial h}{\partial t} + v(t, h, y)\frac{\partial h}{\partial y} = u(t, h, y), \tag{11}$$

where $u(t, g, y)$, $u(t, h, y)$, $v(t, g, y)$ and $v(t, h, y)$ are the velocity components at the free surfaces.

The dynamic boundary conditions on the surfaces are based on the continuity of stress:

$$\sigma \cdot \mathbf{n}_g = -p_g \mathbf{n}_g + \gamma \frac{1}{R_g}\mathbf{n}_g, \tag{12}$$

$$\sigma \cdot \mathbf{n}_h = -p_h \mathbf{n}_h + \gamma \frac{1}{R_h}\mathbf{n}_h, \tag{13}$$

where

$$\sigma = -p\mathbf{I} + \mathbf{T}, \tag{14}$$

is the Cauchy stress tensor, $\mathbf{n}_g$, $\mathbf{n}_h$ are the unit normals to the free surfaces (see Figure 1), p_g, p_h are the ambient pressures around the free surfaces, $\Delta p = p_g - p_h$ is the prescribed driving pressure difference, γ is the coefficient of surface tension and R_g, R_h are the principal radii of curvature of the interfaces,[25]

$$R_g = \left[1 + \left(\frac{\partial g}{\partial y}\right)^2\right]^{3/2} \Big/ \frac{\partial^2 g}{\partial y^2}, \tag{15}$$

$$R_h = \left[1 + \left(\frac{\partial h}{\partial y}\right)^2\right]^{3/2} \Big/ \frac{\partial^2 h}{\partial y^2}, \tag{16}$$

Additional boundary conditions are needed at the walls. We adopt the no-slip boundary condition and no-penetration condition at the two parallel walls. That is

$$\mathbf{v}(t, x, 0) = \mathbf{v}(t, x, L) = \mathbf{0} \tag{17}$$

To close the set of equations (7)–(9), appropriate initial conditions are required. At time $t = 0$, the fluid velocity is zero, $\mathbf{v}(0, x, y) = \mathbf{0}$, as well as the stress $\tau = \mathbf{0}$ and $p = 0$. At time $t > 0$, the driving pressure p_g is applied at the internal free surface $g(t, y)$. On the external free surface $h(t, y)$, we maintain a zero pressure, so that $p_h = 0$. This causes the material to flow.

3. SOLUTION PROCEDURE

The finite element method is a powerful method for non-linear problems. This method has significant advantages in handling complex geometries, including free surfaces. Another major advantage of this method is that the natural boundary conditions on the surface are easily applied. This is important because, when formulating the finite element equations, a surface integral is obtained. Although each constitutive model may vary considerably from the other, the numerical solution procedures all follow the same major steps.

The method may be summarized as follows: the numerical calcuation proceeds in times from given initial data and an initial finite element mesh. The unknown flow field is interpolated by finite element shape functions defined on a continuously deforming mesh. The displacement of the free surfaces is unknown *a priori*, but is determined at each time step by the kinematic equation with the newly calculated unknown field. At each time step, the mesh is deformed to follow the motion of the free surfaces but preseves the initial topology of the element layout. This mesh motion is properly accounted for in the formulation of the discretized problem.

3.1. The finite element method on a moving mesh

In this section we apply the Galerkin finite element method to the viscoelastic free surface flow problem formulated in Section 2. A subject of utmost importance in finite element method is the selection of particular element geometries and the definition of the appropriate approximating functions within each element. After the unknown field variable has been expressed in each element in terms of appropriate nodal parameters and interpolation functions, the derivation of the element equations according to the Galerkin residual method follows a well-established procedure.

Inspection of equations (7)–(9) reveals the implicit character of the stress–strain relation. This prevents the direct elimination of $\mathbf{T}$ in the momentum equation (7) and requires the use of a mixed numerical technique in which extra-stress, together with velocity and pressure are basic unknowns.

Let us define approximations of the finite element type for the unknowns:

$$\mathbf{v}(\mathbf{x}, t) = \sum_{i=1}^{n} \mathbf{V}^i(t)\psi_i, \tag{18}$$

$$\mathbf{T}(\mathbf{x}, t) = \sum_{j=1}^{n} \mathbf{T}^j(t)\phi_j, \tag{19}$$

$$p(\mathbf{x}, t) = \sum_{k=1}^{m} P^k(t)\phi_k \tag{20}$$

where $\mathbf{V}^i$, $\mathbf{T}^j$ and P^k are unknown time-dependent nodal values, while ψ_i, ϕ_j represent shape functions. Since nodal motion is allowed, the shape functions become implicit functions of time through the location of the nodes

$$\psi_i = \psi_i(\mathbf{x}, \mathbf{X}_m(t)), \quad \phi_j = \phi_j(\mathbf{x}, \mathbf{X}_m(t)),$$

where the $\mathbf{X}_m$ are nodal position vectors. In the present simulation, we use isoparametric nine-node quadrilateral elements to discretize the flow domain. In equations (19) and (20) the stress and pressure are given by bi-linear polynomials on the parent elements, while the velocity in (18) is approximated by bi-quadratic polynomials. As we shall see, the functions for moving surfaces are consistently interpolated by quadratic polynomials.

The weak forms of the conservation and stress equations are obtained using the divergence theorem and introducing the natural boundary conditions. A surface integral involves the traction at the walls and free surfaces. Upon insertion of conditions (12) and (13), one ends up with terms like R_g and R_h containing the second order derivatives of free surface functions. Such a degree of regularity, however, is avoided through integration by parts along the free surfaces.[26]

Special care must be taken in the evaluation of time derivatives when the Galerkin procedure is used

on a moving mesh.[22] To illustrate this, we focus on the term $\partial \mathbf{T}/\partial t$, which is given by

$$\frac{\partial \mathbf{T}}{\partial t} = \sum_j \frac{d\mathbf{T}^j(t)}{dt}\phi_j + \sum_j \mathbf{T}^j(t)\frac{\partial \phi_j}{\partial t}. \tag{21}$$

Consider the isoparametric transformation used to perform the integration over a deforming element:

$$\mathbf{x}(\xi, \eta, t) = \sum_m \mathbf{X}_m(t)\psi_m(\xi, \eta), \tag{22}$$

Here $\mathbf{X}_m$ are global nodal coordinates and ψ_m are the shape functions defined on the parent element in (ξ, η) space. Since the (ξ, η) space does not deform with time, the differentiation of the isoparametric transformation with respect to time gives

$$\frac{d\mathbf{x}}{dt} = \sum_m \frac{d\mathbf{X}_m}{dt}\psi_m(\xi, \eta) \equiv \mathbf{v}^e, \tag{23}$$

where $\mathbf{v}^e$ will be referred to as the element velocity. Since the shape function ϕ_j in (ξ, η) space does not depend on time, one has

$$\left.\frac{d\phi_j}{dt}\right|_{(\xi,\eta)} = 0 = \frac{\partial \phi_j}{\partial t} + \left(\sum_m \frac{d\mathbf{X}_m}{dt}\psi_m\right) \cdot \nabla \phi_j. \tag{24}$$

This equation provides a simple expression for $\partial \phi_j/\partial t$. Now we can write (21) as

$$\frac{\partial \mathbf{T}}{\partial t} = \sum_j \frac{d\mathbf{T}^j(t)}{dt}\phi_j - \mathbf{v}^e \cdot \sum_j \mathbf{T}^j(t)\nabla \phi_j. \tag{25}$$

Consequently, the material derivative of T becomes

$$\frac{D\mathbf{T}}{Dt} = \sum_j \frac{d\mathbf{T}^j(t)}{dt}\phi_j + (\mathbf{v} - \mathbf{v}^e) \cdot \nabla \mathbf{T}. \tag{26}$$

Similarly,

$$\frac{D\mathbf{v}}{Dt} = \sum_i \frac{d\mathbf{v}^i(t)}{dt}\psi_j + (\mathbf{v} - \mathbf{v}^e) \cdot \nabla \mathbf{v}. \tag{27}$$

It is observed that the treatment of the remaining terms, in particular the spatial derivatives, remains the same as that in the case of a fixed mesh; only the terms involving the time derivative need be treated as above.

Now let us evaluate the element velocity $\mathbf{v}^e$. The motion of the nodes is related to the displacement of the free surfaces. In this case, the element velocity field generally differs from the fluid velocity. Suppose that the nodal coordinates for element e, at times t_{n-1} and t_n, are given, respectively, by

$$\mathbf{X}_m^{(n-1)} = \left(X_m^{(n-1)}, Y_m^{(n-1)}\right), \quad \mathbf{X}_m^{(n)} = \left(X_m^{(n)}, Y_m^{(n)}\right).$$

The x co-ordinates are tied to the solution at the free boundaries (and their middle points for the interior discretization nodes), while the y co-ordinates are kept fixed. If we use a backward difference method for the time derivatives, then

$$\frac{dX_m}{dt} = \frac{X_m^{(n)} - X_m^{(n-1)}}{\Delta t_n}, \quad \frac{dY_m}{dt} = 0,$$

then we may write

$$\mathbf{v}^e = \begin{pmatrix} u^e \\ v^e \end{pmatrix} = \begin{pmatrix} \sum_m \dfrac{\mathrm{d}X_m}{\mathrm{d}t}\psi_m \\ \\ \sum_m \dfrac{\mathrm{d}Y_m}{\mathrm{d}t}\psi_m \end{pmatrix}$$

$$= \begin{pmatrix} \sum_m (X_m^{(n)} - X_m^{(n-1)})\psi_m/\Delta t_n \\ 0 \end{pmatrix}. \tag{28}$$

We recognize as a special case the conventional Galerkin method on a fixed mesh when $\mathbf{v}^e = \mathbf{0}$.

The final set of non-lineare algebraic equations, resulting from the finite element discretization and an implicit backward finite difference scheme, involves matrix coefficients which are evaluated using Gauss integration quadrature. The non-linearities in the nodal variables are only of the quadratic type, which facilitates considerably the implementation of the Newton–Raphson procedure.

3.2. Determination of free surfaces location

We determine the motion of the free surfaces by solving the kinematic conditions (10) and (11) in their weak Galerkin forms. The finite element discretization in this case is somewhat less obvious than that of the conservation and constitutive equations, and therefore is given here in more details. We define a one-dimensional finite element approximation for the free boundary functions

$$g(t,y) = \sum_l G^l(t)\beta_l(y), \quad h(t,y) = \sum_l H^l(t)\beta_l(y), \tag{29}$$

where β_l is a quadratic polynomial in y.

The one-dimensional mesh is obtained by projecting each free surface node in two-dimensional mesh for flow field on the y-axis. The weak forms of the discretized kinematic conditions read

$$\int_0^L \beta_l\left(\frac{\partial g}{\partial t} + v(t, g^{(n-1)}, y)\frac{\partial g}{\partial y} - u(t, g^{(n-1)}, y)\right)\mathrm{d}y = 0, \tag{30}$$

$$\int_0^L \beta_l\left(\frac{\partial h}{\partial t} + v(t, h^{(n-1)}, y)\frac{\partial h}{\partial y} - u(t, h^{(n-1)}, y)\right)\mathrm{d}y = 0, \tag{31}$$

where u, v are the approximated velocity components evaluated at the free surfaces. Note that the two-dimensional shape functions, when restricted to the boundaries become of the following form

$$\psi_1(h^{(n-1)}, y) = \beta_1(y), \quad \psi_4(h^{(n-1)}, y) = \beta_2(y), \quad \psi_7(h^{(n-1)}, y) = \beta_3(y),$$

$$\psi_2(h^{(n-1)}, y) = \psi_3 = \psi_5 = \psi_6 = \psi_8 = \psi_9 = 0, \tag{32}$$

$$\psi_3(g^{(n-1)}, y) = \beta_1(y), \quad \psi_6(g^{(n-1)}, y) = \beta_2(y), \quad \psi_9(g^{(n-1)}, y) = \beta_3(y),$$

$$\psi_1(g^{(n-1)}, y) = \psi_2 = \psi_4 = \psi_5 = \psi_7 = \psi_8 = 0. \tag{33}$$

We substitute for g and h from (29), and u and v from (18), into (30) and (31), and use finite difference in time, to obtain

$$\left(\frac{1}{\Delta t_n} r_{ij} + V^{3k-2} s_{ijk}\right) H^j = \frac{1}{\Delta t_n} r_{ij} H^{j(n-1)} + U^{3j-2} r_{ij}, \tag{34}$$

$$\left(\frac{1}{\Delta t_n} r_{ij} + V^{3k} s_{ijk}\right) G^j = \frac{1}{\Delta t_n} r_{ij} G^{j(n-1)} + r_{ij} U^{3j}. \tag{35}$$

where, for simplicity, we have introduced the following tensors

$$r_{ij} = \int_0^L \beta_i \beta_j \mathrm{d}y, \quad s_{ijk} = \int_0^L \beta_i \beta_{j,y} \beta_k \mathrm{d}y. \tag{36}$$

The solution from (34) and (35) will be used to locate the boundary nodes in the new mesh for flow field. The internal node motion remains to be defined. We fix the y co-ordinates of nodes and choose the middle position of the two moving boundaries in the x-direction as x co-ordinates for all internal nodes, i.e.

$$x_i(t) = \tfrac{1}{2}(g^i(t) + h^i(t)), \quad y_i(t) = \text{constants}. \tag{37}$$

From the Galerkin discretization and an implicit finite difference scheme for the time derivative, the governing equations (7)–(9) and kinematic conditions (10) and (11) lead to two sets of algebraic equations which may be cast in the form

$$\mathbf{F}(\mathbf{V}, \mathbf{T}, \mathbf{P}; \mathbf{G}, \mathbf{H}) = \mathbf{0}, \tag{38}$$

$$\mathbf{S}(\mathbf{G}, \mathbf{H}; \mathbf{V}) = \mathbf{0}, \tag{39}$$

where **V**, **T**, **P**, **G**, **H** are the vectors of nodal values of flow fields and the free surfaces respectively. The free surface variables **G**, **H** appear in (38) through the boundary conditions at the interface and the mesh.

The solution algorithm is a modification of the one used to solve the problem with one free surface.[1] We will solve the systems (38) and (39) in an uncoupled fashion. From the knowledge of the locations of the free surfaces and the flow field at a discrete value of time t_{n-1}, we predict the free surface locations, stress and velocity fields at time t_n. Then we solve (38) on the predicted flow domain in terms of **V**, **T** and **P**. Finally we correct the locations of the free surfaces by solving (39) with the new velocity field. For further details on the algorithm see Reference 26.

4. NUMERICAL RESULTS

In this section, we examine the influence of surface tension, fluid inertia and elasticity. We begin by examining the flow of a Newtonian fluid. This will constitute a reference basis to be compared to the flow of viscoelastic fluids. While the formulation and numerical integration procedure, discussed in the previous chapters, cover the flow of an Oldroyd-B fluid, the results in the present chapter are mainly centered around the upper-convected Maxwellian fluid. The investigation of fluid retardation is not expected to give significant additional physical insight.

All subsequent numerical results are reported in dimensionless quantities. The reference length is taken as L and time as $\sqrt{L^2\rho/\Delta p}$. There are three important dimensionless groups in the present formulation, namely the Reynolds number, the Weber number and the Deborah number. Another dimensionless group, namely the aspect (height to thickness) ratio is also important. Its effect, however, will not be considered in this work.

The effect of inertia is determined through the value of the Reynolds number, *Re*, which is given by

$$Re = \frac{\sqrt{\rho \Delta p}(R_2 - R_1)}{\mu_1 + \mu_2}.$$

A measure of surface tension is given by the Weber number, *We*, which is

$$We = \frac{\Delta p (R_2 - R_1)}{\gamma}.$$

Another parameter representing surface tension effect is the capillary number:

$$Ca = We/Re.$$

A measure of the fluid elasticity is given by the Deborah number, *De*, which is the ratio of (typical) relaxation time to hydrodynamic timescale. In this case, we set:

$$De = \frac{\lambda_1}{R_2 - R_1}\sqrt{\frac{\Delta p}{p}}$$

We consider the fluid to be initially contained in a rectangle bounded by two parallel plates and two straight free boundaries. The numerical solution was carried out using mixed nine-node quadrilateral elements, as explained earlier. The fluid has been at rest for all times $t < 0$, thus the initial values for **v**, **T** and p are taken as zero at each node, and the locations of free surfaces are $g(0, y) = -0.5$ and $h(0, y) = 0.5$. For $t \geq 0$, the fluid is driven by the continuously applied pressure difference Δp. At each time step, the conserving domain is remeshed according to the new location of the free surfaces but conserves the same topological layout.

4.1. Effect of inertia

The influence of inertia is depicted from Figure 2 which provides the time evolution of the outer surface at the midpoint with the Reynolds number as the changing parameter. We choose a fluid with viscosity $\mu = 300$ Pas, density $\rho = 100$ kg/m^3 and surface tension coefficient $\gamma = 0{\cdot}028$ dyn/m. This gives $Ca = 32143$, which is kept fixed. The different curves are obtained for a Newtonian fluid by varying the applied pressure in the range 9 Pa $\leqslant \Delta p \leqslant$ 4500 Pa. Correspondingly, the Reynolds number is changed from $Re = 0{\cdot}1$ to 2·24. As expected, the fluid deforms at a faster rate as *Re* increases. A similar behaviour is obtained at the inner surface. Figure 3 displays the evolution of the thickness of the fluid column at $y = 5{\cdot}0$, *Re* as the parameter. Over the time range of the calculation, the thickness has decreased with time. The decreasing rate goes faster as *Re* increases.

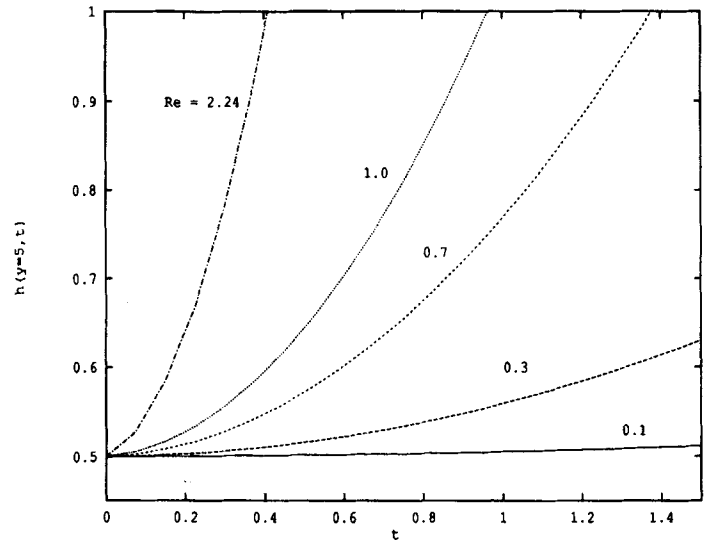

Figure 2. Effect of inertial at the outer surface *h*. Evolution of mid-point for various *Re* values

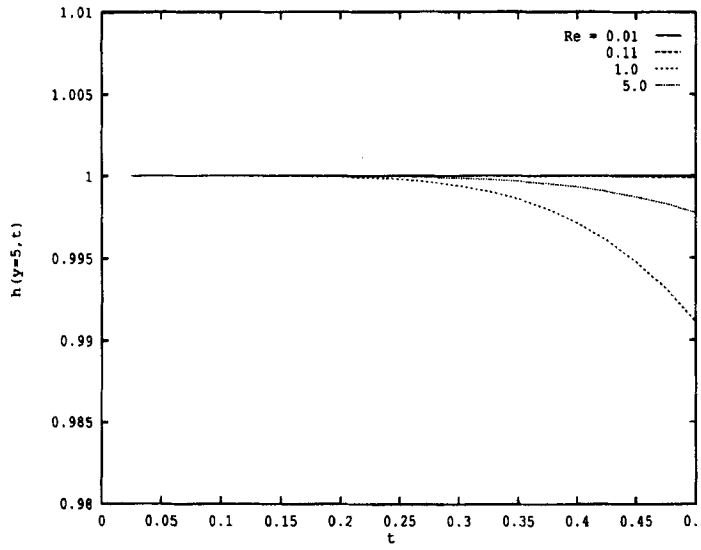

Figure 3. Evolution of thickness of fluid between two surfaces at mid-location

Figure 4 shows the shapes of the two moving free surfaces at different time stages for $Re = 1{\cdot}0$ and without surface tension effect. Both the inner and outer surfaces remain generally flat far away from the boundaries. There is, however, a boundary-layer effect near the walls, which becomes more pronounced with time. The inner surface shows a slight depression in the middle region in comparison with the outer surface. This latter exhibits a strictly flat shape in the middle region. It is interesting to observe from the figure that the concavity does not change with y. This is not always the case as we shall see next.

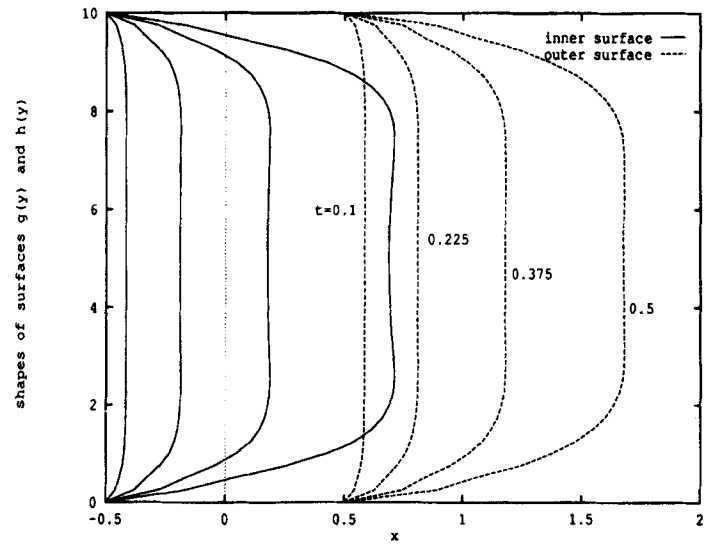

Figure 4. Moving free surfaces at different time stages for $Re = 1{\cdot}0$ in the absence of surface tension

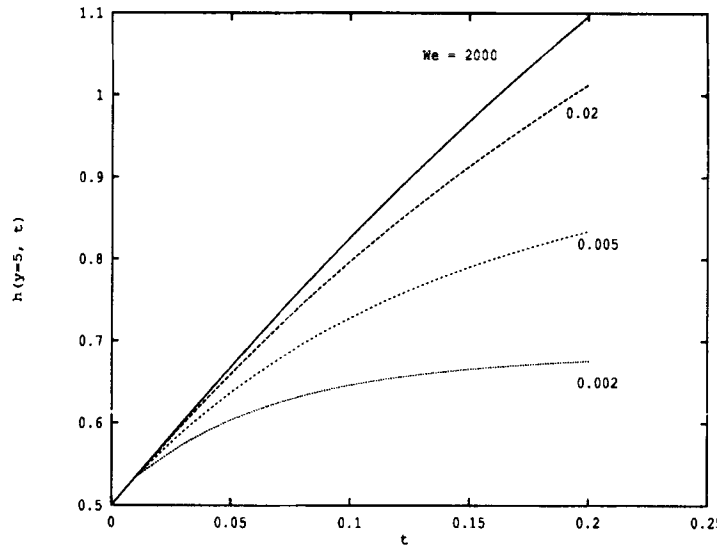

Figure 5. Effect of surface tension at the outer surface h

4.2. *Effect of surface tension*

We examine the effect of surface tension in the case of a Newtonian fluid. In order to speed up the calculation, we limited the results to an inertialess fluid. We set the driving pressure $\Delta p = 20$ Pa, and viscosity $\mu = 500$ Pas, and vary the surface tension coefficient γ in the range $\gamma \in [10^{-2}, 10^{4}]$dyn/m. The value of the aspect ratio is kept as before, i.e. 1:10. In this case, the Weber number $We \in [2 \times 10^{-3}, 2 \times 10^{3}]$.

The influence of We on the evolution of the flow can be depicted from Figures 5 and 6. The evolution of the midpoint of the outer surface is shown in Figure 5. The figure indicates that at the early stages of the motion ($t < 0{\cdot}01$), surface tension does not seem to have any influence. This is expected since the surfaces do not exhibit any significant curvature. At roughly $t > 0{\cdot}01$, the effect of surface tension becomes more evident. The curves in the figure show that as We decreases, the outer surface advances at a slower rate. Thus, surface tension leads to decelerate the flow. A similar trend is observed at the inner surface.

A more detailed picture is obtained from Figure 6, where the actual shapes of the outer and inner surfaces are shown for the highest We value. In this case, the two surfaces exhibit a change in concavity with respect to y. This is in contrast to the situation in Figure 4, where no change in concavity was detected. Recall that in that case, surface tension was neglected. It is then interesting to note that the flattening of the free surfaces in Figure 4 is typical of a polymeric flow when surface tension is indeed negligible. The shapes of the surfaces in Figure 6 are typical of Newtonian fluids.

4.3. *Influence of elasticity*

One of the major motivations behind the present study is the investigation of fluid elasticity in free surface flows. The presence of elasticity as represented by equation (8) is expected to lead to additional numerical difficulties.[12] For this reason, the results in this section are rather limited due to the numerical instabilities encountered, particularly, at a high Deborah number.

We examine the influence of fluid elasticity for an upper-convected Maxwellian fluid ($\mu_2 = 0$) by varying λ_1 and keeping the driving pressure $\Delta p = 150$ Pa, density $\rho = 10$ kg/m^3, thus $Re = 0{\cdot}4$ (fixed).

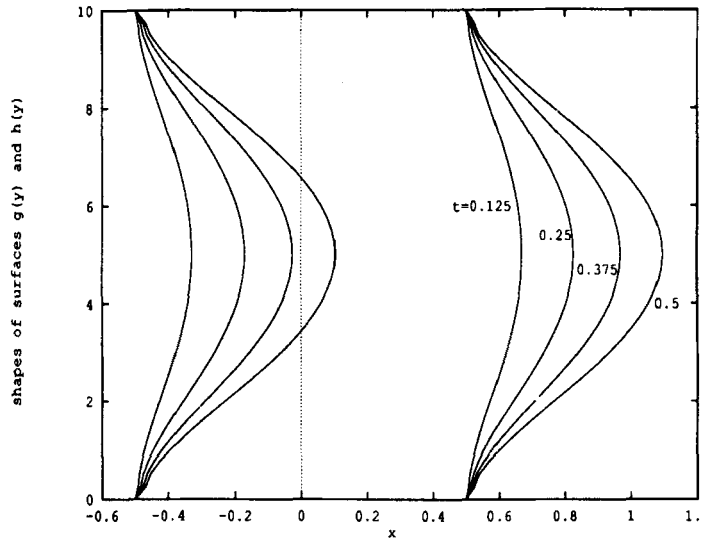

Figure 6. Moving free surfaces at different time stages for $We = 2000$

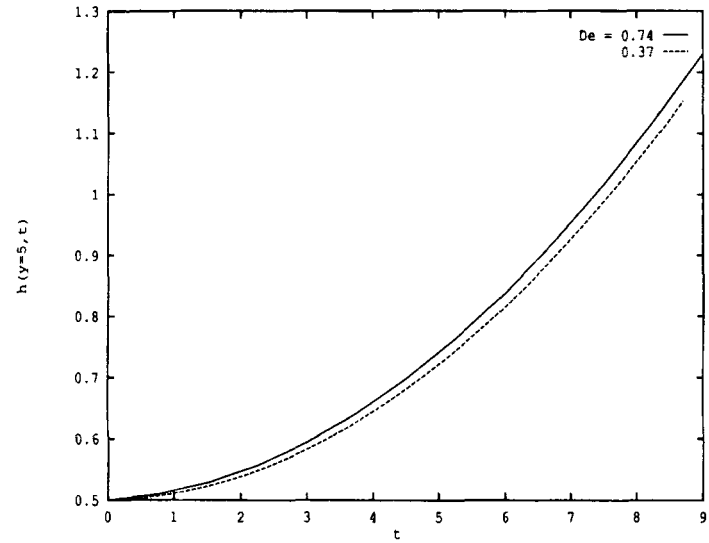

Figure 7. Effect of elasticity at the outer surface h for $Re = 0{\cdot}4$

Surface tension is neglected. Figure 7 shows the evolution of the midpoint at the outer surface as a function of time for $De = 0{\cdot}37$ and $0{\cdot}74$. The figure indicates that fluid elasticity tends to enhance the motion of the fluid. This is in agreement with the results of Khayat.[15]

The onset of numerical instability at higher Deborah number is typically shown in Figure 8. The instability tends to set in first in the vicinity of the rigid boundaries and progress towards the core region. This type of instability is not uncommon in the numerical simulation of free surface flows of viscoelastic fluids.[27] Often, these instabilities are of physical and not numerical nature due to the

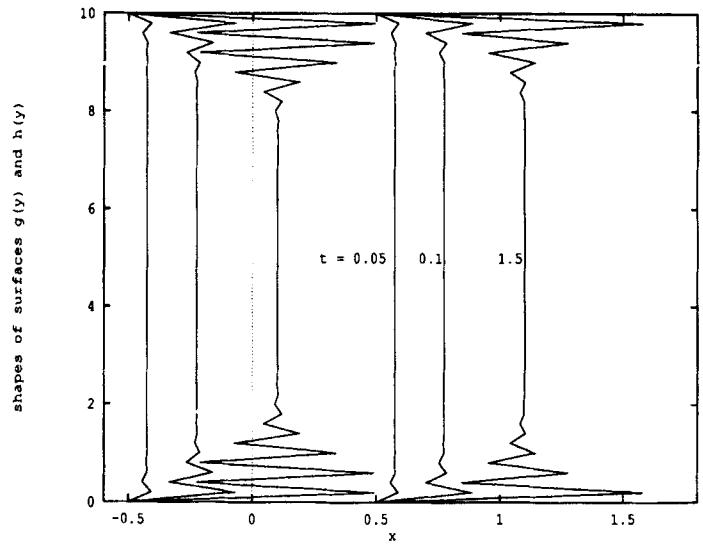

Figure 8. Moving free surfaces at different time stages for $De = 1{\cdot}0$

presence of elasticity. In general, oscillatory (overstable) behaviour, can set in even for statically stressed flows, if the Deborah number is high enough. This has been clearly demonstrated in the case of the inflation of a sphere of viscoelastic material[28] or during the collapse of an air bubbled surrounded by an infinite viscoelastic medium.[29] The flow in these dases is induced by a constant driving pressure. Of course, such an oscillatory motion is absent in Newtonian fluids.

5. CONCLUSION

In this study, the governing equations and boundary conditions for transient flow problems for an Oldroyd-B model with two free surfaces are formulated in two-dimensional space. Newtonian flow is treated as a special case. The flow is assumed incompressible and isothermal. A modified Galerkin method is applied for the numerical solution of two free surface problems in which the spatial mesh deforms in time. The entire study is restricted to simulations in which the finite element topology remains conserved. The problem treated is that of the deformation of a column of fluid under the action of pressure.

An algorithm for the numerical solution of the problem is provided and completely implemented. We have examined the influence of inertia, surface tension and fluid elasticity on the flow by varying one parameter and keeping the remaining parameters fixed. As expected, inertia tends to accelerate the flow. In the absence of surface tension, the inner and outer surfaces do not exhibit any change in concavity. It was found that surface tension tends to oppose the effect of the driving pressure, thus slowing down the flow. Finally, fluid elasticity was found to enhance the rate of deformation.

Over the past decade, much research has been focused on the development of numerical techniques for predicting the flow of viscoelastic fluids in complex geometries. Despite the progress, the numerical prediction of viscoelastic effects in complex geometries has proven to be very difficult in view of the non-linearities related to the fluid memory. Its success is not guaranteed. As we could see in our result in the non-Newtonian case, an oscillatory instability occurred which is difficult to handle. We also realized that the difficulties we observed are not uncommon. This problem remains an open issue. The present work constitutes only a modest attempt in solving transient free surface flows of viscoelastic fluids as they arise in practice. The formulation, in its present form, is rather limited with

regard to problems involving continuously deforming fluids over a long duration. In such problems, the free surface tends to come in contact with the bounding cavity walls due to the fountain flow effect. However, the present formulation can be extended by incorporating appropriate contact conditions at the intersection of free surface and solid wall. In this case, a contact angle may be prescribed or the slip condition may be imposed at the contact node. As it stands, the present method may be directly applicable to problems in blow molding and gas assisted injection molding in cases where the polymer does not deform considerably.

REFERENCES

1. R. Keunings, An algorithm for the simulation of transient flows with free surfaces. *J. Comp. Phys.*, **62**, 199–220 (1986).
2. R. W. Yeung, Numerical methods in free-surface flows. *Ann. Rev. Fluid Mech.*, **14**, 395–442 (1982).
3. T. C. Jue and B. Ramaswamy, Cavity natural convection with a deformable free surface. In *Advances in Finite Element Analysis in Fluid Dynamics*, vol. 137, pp. 95–105, ASME, 1992.
4. C. L. Tucker, *Computer Modeling for Polymer Processing*. Hanser Verlag, Munich, 1988.
5. D. G. Wilson, A. D. Solomon, and P. T. Boggs, *Moving Boundary Problems*. Academic Press, 1978.
6. J. Crank, *Free and Moving Boundary Problems*. Oxford Press, 1984.
7. J. M. Floryan and H. Rasmussen, Numerical methods for viscous flows with moving boundaries. *Appl. Mech. Rev.*, **42**, 323–341 (1989).
8. J. R. A. Pearson and C. J. S. Petrie, The flow of a tubular film. *J. Fluid Mech.*, **40**, 1–19 (1970).
9. M. B. Bush, R. I. Tanner, and N. Phan-Thien, A boundary element investigation of extrudate swell. *J. Non-Newt. Fluid Mech.*, **18**, 143 (1985).
10. A. J. Poslinski and J. A. Tsamopoulos, Nonisothermal parison inflation in blow molding. *AIChE J.*, **36**, 1837–1850 (1990).
11. D. Shah, Gas injection molding: current practices. *SPE Antec*, p. 1494, 1991.
12. M. J. Crochet, Numerical simulation of viscoelastic flow: a review. *Rubber Chemistry Technology*, **62**, 426–455 (1989).
13. R. Keunings, Progress and challenges in computational rheology. *Rheol. Acta*, **29**, 556–570 (1990).
14. R. Keunings, Numerical methods for memory fluids: a critical survey. In *Numerical Methods in Laminar and Turbulent Flow*, pp. 1141–1152, 1987.
15. R. E. Khayat, Perturbation solution to planar flow of a viscolelastic fluid with two moving free boundaries. *Quart. J. Mech. Appl. Math.*, **47**, 341–365 (1994).
16. K. J. Ruschak, A method for incorporating free boundaries with surface tension in finite element fluid flow simulators. *Int. J. Num. Meth. Eng.*, **15**, 639 (1980).
17. H. S. Kheshgi and L. E. Scriven, Penalty finite element analysis of time-dependent two-dimensional free surface film flows. In *Proceedings of the Forth International Symposium on Finite Element Methods in Flow Problems*, Tokyo, 1982.
18. R. E. Nickell, R. I. Tanner, and B. Caswell, The solution of viscous incompressible jet and free-surface flows using finite-element methods. *J. Fluid Mech.*, **65**, 189–206 (1974).
19. G. Ryskin and L. G. Leal, Numerical solution of free-boundary problems in fluid mech. *J. Fluid Mech.*, **148**, 1–47 (1984).
20. Y. Zhang, and J. I. D. Alexander, Surface tension and buoyancy-driven flow in a non-isothermal liquid bridge. *Int. J. Numer. Meth. Fluids*, **14**, 197–215 (1992).
21. E. T. Bullister, L. W. Ho, and E. M. Ronquist, Accurate calculation of free surface flows using the spectral element method. In *Advances in Finite Element Analysis in Fluid Dynamics*, vol. 137, ASME, 1992.
22. D. R. Lynch, Unified approach to simulation on deforming elements with application to phase change problems. *J. Comp. Phys.*, **47**, 387 (1982).
23. D. R. Lynch and W. G. Gray. Finite element simulation of flow in deforming regions. *J. Comp. Phys.*, **36**, 135 (1980).
24. R. B. Bird, R. C. Armstrong, and O. Hassager. *Dynamics of Polymeric Liquids*, vol. 1. Wiley, New York, 2nd edn, 1987.
25. V. G. Levich. *Physicochemical Hydrodynamics*. Prentice-Hall, Englewood Cliffs. N.J., 1962.
26. W. Mao. Numerical simulation of transient viscoelastic flows with two free surfaces. Master's thesis, Dept. of Mathematics and Statistics, McGill University, Montreal, Canada, 1994.
27. A. J. Poslinski. Finite element analysis of the inflation and cooling stages in blow moding operations. PhD thesis, Dept of Chemical Engineering, State University of New York at Buffalo, Buffalo, N.Y., 1990.
28. R. E. Khayat and A. Garcia-Rejon. Uniaxial and biaxial unsteady inflations of a viscoelastic material. *J. Non-Newt. Fluid Mech.*, **43**, 31–59 (1992).
29. H. S. Fogler and J. D. Goddard. Collapse of spherical cavities in viscoelastic fluids. *Phys. Fluids*, **13**, 1135–1141 (1970).